NUMERICAL METHODS FOR SIMULATING THE FLOW OVER AN AIRFOIL COVERED WITH A THIN LAYER OF LIQUID

O.J. Boelens, P.J.J. Moeleker, H. de Jong and H.W.M. Hoeijmakers

Department of Aerospace Engineering
Delft University of Technology
Kluyverweg 1, 2629 HS Delft, The Netherlands

Abstract

De-icing and anti-icing fluids protect an aircraft from ice, snow or frost accumulation. These fluids, however, may have adverse effects on the aircraft aerodynamics, thought to be caused by the boundary layer thickening due to the formation of surface waves. In this paper two aspects of this problem are dealt with. The incompressible time-dependent boundary-layer flow has been calculated using a finite-volume formulation. The truncated definition of the stream function was used to simplify the governing equations. A computational grid was generated utilizing the similarity transformations. The method was validated and used to determine the effect of solid wall roughness. It has been found that the addition of solid wall roughness results in a substantial thickening of the boundary layer.
Furthermore, the linear hydrodynamic stability of the flow of a gas over a non-Newtonian power-law fluid has been investigated using the theory of small perturbations. A virtual interface was introduced to take care of the boundary conditions at infinity. The resulting set of equations was solved using Chebyshev polynomials and the QZ-algorithm. For a non-Newtonian power-law liquid sheared by a Newtonian gas two unstable mode were obtained, i.e the Blasius mode and the interfacial mode. The energy distributions throughout the layers were investigated to determine the origin of the instability.

Introduction

Since 1930, it has been general practice to use water-glycol mixtures to protect an aircraft on the ground from ice, snow or frost accumulation. However, in the mid-1980's it appeared that the (non-Newtonian) fluids used to de-/anti-ice the aircraft might have an adverse effect on the aircraft aerodynamics during take-off. The presence of these fluids results in a lift loss, a drag increase and a decrease of the stall angle. Experimental investigations[2],[4],[8] have shown that during take-off, before the fluid is finally blown off the surface, the fluid surface roughens, i.e. waves are formed. It was hypothesized that the boundary-layer thickened due to the surface roughness in a manner similar to the effect due to solid wall roughness. The flow configuration is shown in Figure 1.

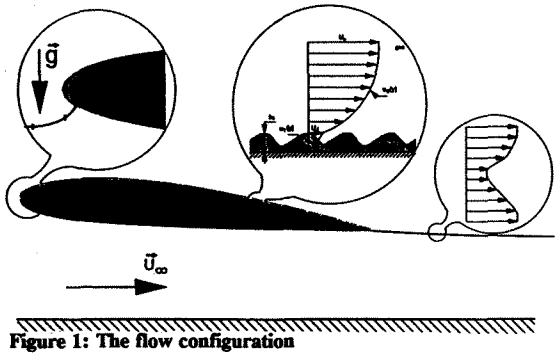

Figure 1: The flow configuration

In order to have a simple, cost-effective aerodynamic acceptance test for de-/anti-icing fluids in a small cooled wind tunnel, it was proposed to substitute the upper surface of the airfoil by a flat surface. Experiments were performed to determine the correlation between the lift loss on a three-dimensional wing and the flow over a flat surface[2]. For determining the time-dependent air boundary-layer thickness, a method based on the wind-tunnel blockage method was used.
This paper deals with two aspects which are of interest for the problem of boundary-layer thickening due to the formation of waves on a (non-Newtonian) liquid subjected to an airflow. In the first part a method will be discussed to calculate the time-dependent boundary-layer over a flat plate. A turbulence model was incorporated to enable calculations of a turbulent boundary-layer and investigate the effect of wall roughness. The second part of the paper deals with the linear hydrodynamic stability analysis of a non-Newtonian power-law fluid sheared by a gas flow. This analysis is performed in order to determine whether or not instabilities will arise at the gas-liquid interface.

Computational method for a gas boundary-layer

From experimental investigations it has been concluded that the adverse aerodynamic effects of de-/anti-icing fluids are mainly due to the thickening of the boundary-layer caused by the occurrence of surface waves. To investigate this phenomenon a cell-vertex finite-volume method was used to solve the two-dimensional unsteady boundary-layer equations. The method used is a modification of the method of Loyd and Murman[5] for solving the two-dimensional steady compressible boundary-layer equations. An algebraic turbulence model was incorporated to investigate the effect of wall roughness.

Governing equations

The governing equations for the unsteady two-dimensional incompressible boundary-layer are Prandtl's boundary-layer equations. The continuity and momentum equations for an arbitrary control volume S (boundary ∂S) in integral form are

$$\oint_{\partial S} u dy - \oint_{\partial S} v dx = 0$$

$$\frac{\partial}{\partial t}\int_S \int u dS + \oint_{\partial S} u^2 dy - \oint_{\partial S} uv dx = -\oint_{\partial S} \frac{p}{\rho} dy - \oint_{\partial S} \frac{\tau}{\rho} dx$$

respectively, where x is the arclength along and y is the distance normal to the surface. $u(x,y,t)$ and $v(x,y,t)$ are the tangential and normal (mean) velocity components, $p(x,t)$ is the given static pressure, ρ is the density and $\tau(x,y,t)$ is the shear stress defined by

$$\tau = \mu \frac{\partial u}{\partial y}$$

with $\mu = \mu_l + \mu_t$. Here μ_l and μ_t are the molecular viscosity and the turbulent viscosity, respectively.

Stream function formulation

A stream function $\psi(x,y,t)$ is introduced such that the continuity equation is satisfied, i.e.

$$(u,v) = \left(\frac{\partial \psi}{\partial y}, -\frac{\partial \psi}{\partial x}\right) \qquad (1)$$

Since gridlines are perpendicular to the surface at each streamwise station, $dx = 0$ along gridlines in the direction normal to the wall. In that case the continuity equation may be replaced by the truncated definition of the stream function

$$d\psi = u dy_{x=constant}$$

When this definition is applied at each streamwise station, one obtains the following set of equations

$$d\psi = u dy_{x=constant}$$

$$\frac{\partial}{\partial t}\oint_{\partial S} \psi dx = \oint_{\partial S} u d\psi + \oint_{\partial S} \frac{p}{\rho} dy + \oint_{\partial S} \frac{\tau}{\rho} dx$$

$$\tau = \mu \frac{\partial u}{\partial y}$$

where it has been used that

$$u^2 dy - uv dx = u d\psi$$

Non-dimensionalization

All variables are non-dimensionalized using the free stream quantities U_∞, ρ_∞, and some characteristic length L, i.e.

$$x' = \frac{x}{L} \qquad y' = \frac{y}{L} \qquad t' = \frac{U_\infty t}{L}$$

$$u' = \frac{u}{U_\infty} \qquad v' = \frac{v}{U_\infty}$$

$$p' = \frac{p}{\rho_\infty U_\infty^2} \qquad \psi' = \frac{\psi}{U_\infty L} \qquad \tau' = \frac{\tau}{\rho_\infty U_\infty^2}$$

$$\mu_l' = \frac{\mu_l}{\rho_\infty U_\infty L} = \frac{1}{Re} \qquad \mu_t' = \frac{\mu_t}{\rho_\infty U_\infty L} \qquad \rho' = \frac{\rho}{\rho_\infty}$$

The form of the non-dimensional governing equations is identical to that of the dimensional equations. Note that the Reynolds number is contained in the dimensionless viscosity. For convenience the primes are dropped and henceforth reference is made to the non-dimensional form only.

Turbulence model

For the turbulent boundary-layer flow the algebraic eddy viscosity formulation of Cebeci and Smith was used[1],[9]. This model represents a zero-equation closure, i.e. the turbulent shear stress is evaluated through a set of algebraic equations. The eddy viscosity is given by a two-layer model, in which the turbulent viscosity in the inner region is based on Van Driest's approach, and in the outer region on a velocity defect approach (non-dimensional formulation)

$$\mu_{ti} = \rho L_m^2 \left|\frac{\partial u}{\partial y}\right| \gamma_{tr}, \qquad 0 < y < y_c$$

$$\mu_{to} = \alpha \rho U_\infty \delta^* \gamma_{tr} F_{Kleb}(y,\delta), \quad y_c < y < y_e$$

where L_m is the mixing length, δ^* is the kinematic displacement thickness, γ_{tr} is an intermittency factor, α is a function of the Reynolds number, and $F_{Kleb}(y,\delta)$ is the Klebanoff intermittency function. y_c is the distance from the wall at which the turbulent viscosity of the inner region equals that of the outer region.

The mixing length L_m is proportional to the distance y from the wall, $L=\kappa y$, where κ is

$$\kappa=\kappa_0(1-e^{-\frac{y}{A}})$$

which incorporates the Van Driest modification for the mixing length, where the Von Kármán constant κ_0 equals 0.4 and A is the Van Driest damping parameter given by

$$A=A^+\frac{\nu}{N}\left[\frac{\tau_w}{\rho}\right]^{-\frac{1}{2}}$$

where $A^+=26$, and

$$N=\sqrt{1-11.8P^+}\ , \qquad P^+=\left[\frac{\nu_e U_e}{U_\tau^3}\right]\frac{dU_e}{dx}\frac{\mu_w}{\mu_e}$$

and the friction velocity U_τ is

$$U_\tau=\left[\frac{\tau_w}{\rho}\right]^{\frac{1}{2}}$$

Here the subscripts w and e indicate that the property should be taken at the solid wall and at the edge of the boundary layer, respectively.
The above formulae, used with $\alpha=0.0168$ give accurate results for high Reynolds numbers. For

$$Re_\theta=\frac{U_\infty\theta}{\nu}<5000$$

one should use

$$\alpha=\alpha_0\frac{1+\pi_0}{1+\pi}$$

where

$$\pi=\pi_0[1-\exp(-0.243\sqrt{z_1}-0.298z_1)]\ , \qquad z_1=\frac{Re_\theta}{425}-1$$

and $\pi_0=0.55$ and $\alpha_0=0.0168$. Here θ denotes the momentum thickness.
In order to incorporate surface roughness in the turbulence model, the distance y from the wall may be modified as $y+\Delta y$ where Δy is a function of an equivalent sand-grain roughness k_s. In terms of dimensionless quantities k_s^+ and Δy^+, one has

$$\Delta y^+=\frac{\Delta y U_\tau}{\nu}=0, \qquad 0<k_s^+=\frac{k_s U_\tau}{\nu}\le 5$$

$$\Delta y^+=0.9\left[\sqrt{k_s^+}-k_s^+e^{-\frac{k_s^+}{6}}\right], \qquad 5<k_s^+\le 70$$

$$\Delta y^+=0.7(k_s^+)^{0.58}, \qquad 70<k_s^+\le 2000$$

In order to account for the transitional flow region, the intermittency distribution of Chen and Thyson was used, i.e.

$$\gamma_{tr}=1-\exp\left[-\frac{U_e^3}{G_{tr}\nu^2}Re_{tr}^{-1.34}(x-x_{tr})\int_{x_{tr}}^{x}\frac{d\xi}{U_e}\right]$$

where x_{tr} and Re_{tr} are the location of the onset of transition and the transition Reynolds number, respectively. The empirical factor G_{tr} exerts a major influence on the length of the transition region. Throughout all calculations its value was fixed at 1200.

Grid generation

The grid is constructed using similarity principles. The outer edge of the grid is chosen to be proportional to the incompressible momentum thickness $\theta_{in}(x)$, since in most laminar and turbulent flows that quantity is proportional to the boundary layer thickness[5]. For non-similar flows it may be assumed that the streamwise changes are small, and thus the flow is locally similar. Thus $\theta_{in}(x)$ is calculated using a locally similar approximation.
In the transition region the grid is modified to create a smooth transition from the laminar to the turbulent region.

Initial and boundary conditions

The value of the stream function at the solid wall follows from the definition of the stream function. Integrating this definition from station i-1 to station i, one obtains

$$\psi_i=\psi_{i-1}$$

As initial and inflow condition a sixth-degree polynomial approximation of the Blasius velocity profile was taken for the tangential velocity, i.e.

$$\frac{u}{U_\infty}=2\eta_1-5\eta_1^4+6\eta_1^5-2\eta_1^6, \qquad 0\le\eta_1=\frac{\eta}{6}=\frac{y}{6}\left[\frac{U_\infty}{\nu_\infty x}\right]^{\frac{1}{2}}<1$$

$$=1, \qquad \frac{\eta}{6}\ge 1$$

The normal velocity was taken to be zero at all

points. Using equation (1) the stream function can be calculated at all points of an axial station by integration.

Discretization and time stepping

A second-order cell-vertex finite-volume discretization was adopted. The momentum fluxes through a given cell are calculated by a quadratic representation of the state variables at adjacent nodes.

A five-stage Runge-Kutta scheme ($\alpha_1=1/4$, $\alpha_2=1/6$, $\alpha_3=3/8$, $\alpha_4=1/2$ and $\alpha_5=1 \Rightarrow CFL_{max}=2\sqrt{2}$) which is second-order accurate in Δt, was used to advance the momentum equation in time.

Results

Using the techniques described in the preceding paragraphs, calculations of the flow over a flat plate have been performed to validate the computational method and to investigate the effect of solid-wall roughness.

The length of the flat plate was taken to be 0.5m. The inflow boundary was taken at $x=0.02$m. The computational grid consisted of 25 stations of 40 nodes each. The laminar calculation has been performed on a 'laminar' grid, all turbulent calculations have been performed on a 'turbulent' grid (see Figure 2).

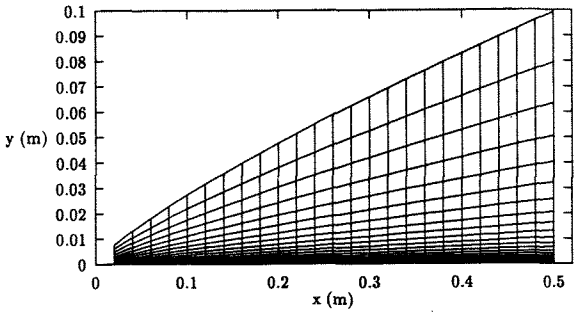

Figure 2: The 'turbulent' computational grid

The gas used was air at a temperature of 0°C , so that $\rho=1.29\text{kgm}^{-3}$ and $\mu=17.1\text{x}10^{-6}\text{kgm}^{-1}\text{s}^{-1}$. The reference length was 1m, and the free stream velocity, i.e. the reference velocity, was 60ms^{-1}. In case of a turbulent flow transition occurred at a transition Reynolds number of $Re_{tr}= 5\text{x}10^5$.

Figure 3 shows the local skin friction coefficient c_f as function of the local Reynolds number Re_x for a laminar flow, a turbulent flow and a turbulent flow with wall roughness. This figure includes the theoretical local skin friction coefficient for a laminar flow

$$c_f=\frac{\tau_w}{\frac{1}{2}\rho U_\infty^2}=\frac{0.664}{Re_x^{\frac{1}{2}}}$$

and the one for a turbulent flow

$$c_f=\frac{\tau_w}{\frac{1}{2}\rho U_\infty^2}=\frac{0.0592}{Re_x^{\frac{1}{5}}}$$

which is valid for Reynolds numbers between $5\text{x}10^5$ and $1\text{x}10^7$. The figure shows good agreement between the theoretical and numerical results. Furthermore it can be seen that the wall roughness results in an increase of the local skin friction.

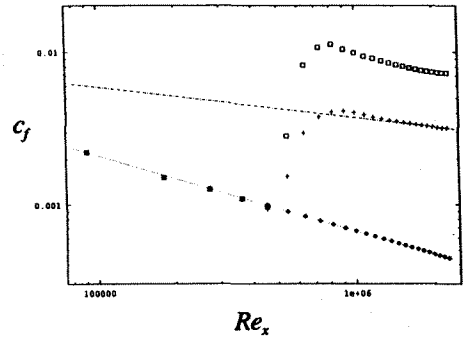

Figure 3: c_f vs Re_x (◇: laminar; +: turbulent; □: turbulent, k_s = $5\text{x}10^{-4}$m)

Figure 4 shows the boundary-layer thickness δ and the displacement thickness δ^* for the turbulent boundary-layer with and without wall roughness.

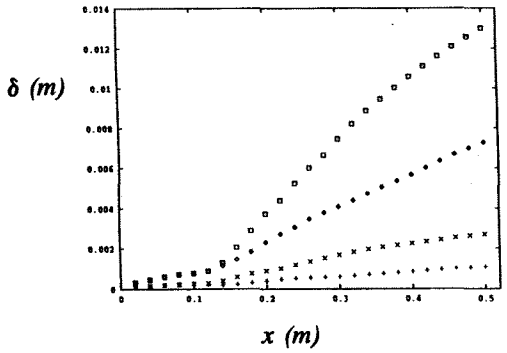

Figure 4: δ, δ^* vs x (◇, +: turbulent; □, x: turbulent, k_s= $5\text{x}10^{-4}$m)

From this figure it is clear that the boundary-layer thickens due to solid wall roughness. At $x=0.5$m the displacement thickness δ is almost doubled due to the solid wall roughness.

Conclusions

The incompressible time-dependent boundary-layer flow has been calculated using a finite-volume formulation. Instead of using similarity transformations to transform the governing equations, explicit use of these transformations has been made to generate the computational grid. The governing equations have been simplified using a truncated definition of the stream function. For turbulent flows the Cebeci-Smith turbulence model was used.

The calculated results show good agreement with theory. The addition of solid wall roughness leads to boundary-layer thickening.

In the introduction it was stated that the fluid surface roughens the surface of the airfoil due to the formation of 'instationary' waves. As the shape of the waves is not exactly known, it is not possible to calculate the effect of these waves on the boundary layer flow. Future research includes the problem of the wave formation and determining the transient wave shape.

Linear hydrodynamic stability analysis

The linear hydrodynamic stability analysis has since long been used as a tool to investigate the initiation of instabilities in a flow. Recent articles on this subject are by Miesen & Boersma[6] and by Yih[10].

The case of a non-Newtonian power-law liquid sheared by a Newtonian gas was investigated by Özgen[7]. In the next paragraphs the equations governing the stability of the flow of a Newtonian fluid on top of a non-Newtonian power-law fluid will be derived as well as the conditions to be imposed at the Newtonian/non-Newtonian interface.

Furthermore, the stability of a model flow will be investigated, where also the perturbation energy distribution will be considered.

The governing equations

For the two-dimensional flow over a horizontal plate of an incompressible, non-Newtonian power-law fluid, the governing Navier-Stokes equations are, in Cartesian coordinates

$$\frac{\partial u}{\partial x}+\frac{\partial v}{\partial y}=0$$

$$\frac{\partial u}{\partial t}+u\frac{\partial u}{\partial x}+v\frac{\partial u}{\partial y}=-\frac{1}{\rho}\frac{\partial p}{\partial x}+\frac{1}{\rho}\frac{\partial \tau_{xx}}{\partial x}+\frac{1}{\rho}\frac{\partial \tau_{xy}}{\partial y}$$

$$\frac{\partial v}{\partial t}+u\frac{\partial v}{\partial x}+v\frac{\partial v}{\partial y}=-\frac{1}{\rho}\frac{\partial p}{\partial y}+\frac{1}{\rho}\frac{\partial \tau_{yx}}{\partial x}+\frac{1}{\rho}\frac{\partial \tau_{yy}}{\partial y}+g$$

where $u(x,y,t)$ and $v(x,y,t)$ are the velocities in the x- and y-direction, respectively, $p(x,y,t)$ denotes the pressure, ρ is the density [kgm^{-3}] and g is the gravitational acceleration [ms^{-1}]. The non-Newtonian stress tensor $\tau(x,y,t)$ is given by

$$\tau=2k\left[2\left(\frac{\partial u}{\partial x}\right)^2+\left(\frac{\partial u}{\partial y}+\frac{\partial v}{\partial x}\right)^2+2\left(\frac{\partial v}{\partial y}\right)^2\right]^{\frac{n-1}{2}}e$$

where k denotes the dimensional consistency constant in the power-law [kgs^{n-2}m^{-1}], n the power-law index and e the rate-of-strain tensor. For a Newtonian fluid n equals 1 and $k=\mu$.

The linear hydrodynamic stability theory assumes that the motion of a fluid can be decomposed into a primary flow component ($O(\epsilon^0)$) and a secondary flow component ($O(\epsilon^1)$), i.e.

$$u(x,y,t)=\hat{u}(x,y,t)+\epsilon\tilde{u}(x,y,t)+O(\epsilon^2)$$
$$v(x,y,t)=\hat{v}(x,y,t)+\epsilon\tilde{v}(x,y,t)+O(\epsilon^2)$$
$$p(x,y,t)=\hat{p}(x,y,t)+\epsilon\tilde{p}(x,y,t)+O(\epsilon^2)$$

Primary flow

Upon assuming an infinite region in the x-direction and a steady primary flow, the primary velocity components in the x- and y-direction can only be a function of y. For a steady flow bounded at one side by a solid wall it follows that

$$\hat{u}(x,y,t)=\hat{u}(y) \qquad \hat{v}(x,y,t)=0 \qquad \hat{p}(x,y,t)=\hat{p}(x,y)$$

It can be shown that the following analysis also holds for flows with a primary velocity profile that varies slightly with x and which has a small non-zero y-component of the velocity, so-called nearly parallel flows[3].

Secondary flow

Substitution of the series expansion and using the primary flow solution yields for the $O(\epsilon^1)$ terms:

$$\frac{\partial \tilde{u}}{\partial x}+\frac{\partial \tilde{v}}{\partial y}=0$$

$$\frac{\partial \tilde{u}}{\partial t}+\hat{u}\frac{\partial \tilde{u}}{\partial x}+\tilde{v}\frac{d\hat{u}}{dy}=-\frac{1}{\rho}\frac{\partial \tilde{p}}{\partial x}+2\frac{k}{\rho}\frac{\partial}{\partial x}\left[\left(\frac{d\hat{u}}{dy}\right)^{n-1}\left(\frac{\partial \tilde{u}}{\partial x}\right)\right]$$
$$+\frac{k}{\rho}\frac{\partial}{\partial y}\left[n\left(\frac{d\hat{u}}{dy}\right)^{n-1}\left(\frac{\partial \tilde{u}}{\partial y}+\frac{\partial \tilde{v}}{\partial x}\right)\right] \qquad (2)$$

$$\frac{\partial \tilde{v}}{\partial t}+\hat{u}\frac{\partial \tilde{v}}{\partial x}=-\frac{1}{\rho}\frac{\partial \tilde{p}}{\partial y}+\frac{k}{\rho}\frac{\partial}{\partial x}\left[n\left(\frac{d\hat{u}}{dy}\right)^{n-1}\left(\frac{\partial \tilde{u}}{\partial y}+\frac{\partial \tilde{v}}{\partial x}\right)\right]$$

$$+2\frac{k}{\rho}\frac{\partial}{\partial y}\left[\left(\frac{d\hat{u}}{dy}\right)^{n-1}\left(\frac{\partial \tilde{v}}{\partial y}\right)\right]$$

These equations are non-dimensionalized using a reference density ρ_{ref}, a reference velocity U_{ref} and a reference length L_{ref}.

Introducing a perturbation stream function according to

$$(\tilde{u},\tilde{v})=(\frac{\partial \psi}{\partial y},-\frac{\partial \psi}{\partial x}) \qquad (3)$$

implicitly satisfies the continuity equation. It is assumed that the stream function can be written as the sum of Fourier modes, as is the pressure. Because the equations governing the secondary flow are linear, only one Fourier mode needs to be considered, which can be expressed as

$$(\psi(x,y,t),p(x,y,t))=(\phi(y),f(y))\ e^{i\alpha(x-ct)} \qquad (4)$$

where $i^2=-1$. The (always positive) non-dimensional wave number α is defined by

$$\alpha=2\pi\frac{L_{ref}}{\lambda}>0$$

where λ is the dimensional wave length. The complex wave speed is $c=c_r+ic_i$, where c_r and c_i are the real and imaginary part of the non-dimensional complex wave speed, respectively. A flow is said to be stable, if for all wave numbers the imaginary part of the complex wave speed is negative. In all other cases, the flow is said to be (linearly) unstable. It should be noted that by introducing the Fourier series in this manner (α real, c complex), one investigates the temporal linear instability problem.

Upon substitution of equations (3) and (4) in equations (2), one obtains

$$-(\hat{u}-c)\phi'+\hat{u}'\phi=\frac{1}{r}f$$

$$-\frac{m}{i\alpha Rer}\left[n\phi'''+(n-2)\alpha^2\phi'\right] \qquad (5)$$

$$-\frac{mn}{i\alpha Rer}(n-1)\left(\frac{\hat{u}''}{\hat{u}'}\right)\left[\phi''+\alpha^2\phi\right]$$

$$(\hat{u}-c)\alpha^2\phi=-\frac{1}{r}f'$$

$$+\frac{i\alpha m}{Rer}\left[(n-2)\phi''+n\alpha^2\phi\right]$$

$$-2\frac{i\alpha m}{Rer}(n-1)\left(\frac{\hat{u}''}{\hat{u}'}\right)\phi'$$

where a prime indicates differentiation with respect to y. The Reynolds number Re, the density ratio r and the viscosity ratio m are defined by

$$Re=\frac{\rho_{ref}U_{ref}L_{ref}}{\mu_{ref}}$$

$$r=\frac{\rho}{\rho_{ref}} \qquad (6)$$

$$m=\frac{k}{\mu_{ref}}\left(\frac{U_{ref}\hat{u}'}{L_{ref}}\right)^{n-1}$$

respectively, where μ_{ref} is a reference viscosity. Elimination of f, i.e. the pressure term, from these equations yields the Orr-Sommerfeld equation for a non-Newtonian power-law fluid

$$\phi^{iv}-2\alpha^2\phi''+\alpha^4\phi-\frac{i\alpha Rer}{nm}\left[(\hat{u}-c)(\phi''-\alpha^2\phi)-\hat{u}''\phi\right]$$

$$+(n-1)\left[2\left(\frac{\hat{u}''}{\hat{u}'}\right)\phi'''\right]$$

$$+\frac{(n-1)}{n}\left[\{n(n-2)\left(\frac{\hat{u}''}{\hat{u}'}\right)^2+n\left(\frac{\hat{u}'''}{\hat{u}'}\right)+4\alpha^2\}\phi''\right]$$

$$+\frac{(n-1)}{n}\left[2(n-2)\left(\frac{\hat{u}''}{\hat{u}'}\right)\alpha^2\phi'\right]$$

$$+(n-1)\left[\{\left(\frac{\hat{u}'''}{\hat{u}'}\right)+(n-2)\left(\frac{\hat{u}''}{\hat{u}'}\right)^2\}\alpha^2\phi\right]=0$$

For $n=1$ this equation reduces to the classical Orr-Sommerfeld equation for the stability of a steady parallel flow.

A non-Newtonian power-law fluid sheared by a gas

Consider two parallel horizontal fluid layers on top of each other with the lower fluid bounded by a fixed wall and the upper fluid stretching to infinity (Figure 5).

The upper (Newtonian, $n=1$) fluid has a stream function ϕ and will be referred to with subscript 1, and the lower (non-Newtonian) fluid has a stream function χ and will be referred to with subscript 2. In the upper fluid the velocity profile will assumed to be

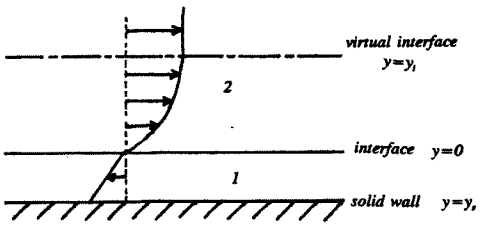

Figure 5: The flow configuration

the (nearly parallel) Blasius velocity profile. It is assumed that the mean thickness of lower layer is constant. In that case the $O(\epsilon^0)$ equations have a solution which is linear for all n if the pressure gradient in the x-direction is zero. All quantities are non-dimensionalized using the free stream properties of the upper fluid, i.e. $\rho_{ref}=\rho_1$, $\mu_{ref}=\mu_1$, $U_{ref}=U_\infty$ and $L_{ref}=L^*$ being the length scale of the Blasius solution

$$L^* = \left(\frac{\mu_1 x}{\rho_1 U_\infty} \right)^{\frac{1}{2}}$$

with x a dimensional location along the flat plate.
For this situation one obtains the following set of Orr-Sommerfeld equations

$$\phi^{iv} - 2\alpha^2\phi'' + \alpha^4\phi - i\alpha Re\left[(\hat{u}_1 - c)(\phi'' - \alpha^2\phi) - \hat{u}_1''\phi\right] = 0$$

$$\left[n\chi^{iv} + 2(n-2)\alpha^2\chi'' + n\alpha^4\chi\right] - \frac{i\alpha Rer}{m}\left[(\hat{u}_2 - c)(\chi'' - \alpha^2\chi)\right] = 0$$

for the upper fluid and the lower fluid, respectively. The density ratio r, the Reynolds number Re and the viscosity ratio m are

$$r = \frac{\rho_2}{\rho_1}$$

$$Re = \frac{\rho_1 U_\infty L^*}{\mu_1}$$

$$m = \frac{k}{\mu_1}\left(\frac{U_\infty}{L^*}\hat{u}_2' \right)^{n-1}$$

respectively. In order to solve this set of fourth-order linear partial differential equations four boundary and four interface conditions are needed, which will be derived in the next paragraphs.

Solid wall boundary conditions

The solid wall boundary conditions follow from the no-slip condition, i.e.

$$(\tilde{u},\tilde{v})(x,y_s,t) = (0,0)$$

where y_s denotes the non-dimensional y-coordinate of the solid wall. Substitution of the series expansion and the stream function definition results in the following two conditions

$$\chi(y_s) = 0$$
$$\chi'(y_s) = 0$$

Interface conditions

The distance between the actual location of the interface and that of the primary interface between the two fluids is indicated by $\eta(x,t)$, where $\eta(x,t)$ is expressed as the following series expansion

$$y = \eta(x,t) = \epsilon\tilde{\eta}(x,t) + O(\epsilon^2)$$

In this expansion it has been assumed that the interface in the primary solution coincides with the line $y=0$, see Figure 5.
The location of the interface is described by

$$\frac{D(y-\eta(x,t))}{Dt} = v - \frac{\partial\eta(x,t)}{\partial t} - u\frac{\partial\eta(x,t)}{\partial x} = 0$$

Substitution of the series expansions, the stream function definition, results upon non-dimensionalizing in

$$\tilde{\eta}(x,t) = \frac{\phi(0)}{c-\hat{u}(0)}e^{i\alpha(x-ct)}$$

The dimensional interface conditions at $y=\eta(x,t)$ are:
a. Continuity of tangential velocity

$$[\![\, u(x,\eta(x,t),t) \,]\!] = 0$$

b. Continuity of normal velocity

$$[\![\, v(x,\eta(x,t),t) \,]\!] = 0$$

c. Continuity of tangential stress

$$[\![\, s_t(x,\eta(x,t),t) \,]\!] = 0$$

d. Continuity of normal stress

$$[\![\, s_n(x,\eta(x,t),t) \,]\!] + \sigma K = 0$$

Here, σ is the surface tension [Nm^{-1}] and K the

curvature of the interface. The dimensional stress components s_t and s_n can be derived from the non-Newtonian power-law stress tensor using the normal and tangent unit vectors along the interface. They are found to be

$$s_t=\frac{2k}{1+\eta_x^2}\left[2\left(\frac{\partial u}{\partial x}\right)^2+\left(\frac{\partial u}{\partial y}+\frac{\partial v}{\partial x}\right)^2+2\left(\frac{\partial v}{\partial y}\right)^2\right]^{\frac{n-1}{2}}\cdot \left[\frac{1}{2}\left(1-\eta_x^2\right)\left(\frac{\partial u}{\partial y}+\frac{\partial v}{\partial x}\right)+2\eta_x\frac{\partial v}{\partial y}\right]$$

$$s_n=-p+\frac{2k}{1+\eta_x^2}\left[2\left(\frac{\partial u}{\partial x}\right)^2+\left(\frac{\partial u}{\partial y}+\frac{\partial v}{\partial x}\right)^2+2\left(\frac{\partial v}{\partial y}\right)^2\right]^{\frac{n-1}{2}}\cdot \left[-\eta_x\left(\frac{\partial u}{\partial y}+\frac{\partial v}{\partial x}\right)+\left(1-\eta_x^2\right)\frac{\partial v}{\partial y}\right]$$

Substitution of the series expansion for p, u and v and the location of the interface $\eta(x,t)$, the definition for the stream function, results upon non-dimensionalizing and collecting $O(\epsilon)$ terms in

a. Continuity of tangential velocity

$$\phi'(0)-\chi'(0)=\frac{\phi(0)}{c-\hat{u}(0)}\left[u_2'(0)-u_1'(0)\right] \qquad (7)$$

b. Continuity of normal velocity

$$\phi(0)-\chi(0)=0 \qquad (8)$$

c. Continuity of tangential stress

$$\phi''(0)+\alpha^2\phi(0)-nm\left(\chi''(0)+\alpha^2\chi(0)\right)=0 \qquad (9)$$

d. Continuity of normal stress

$$\begin{aligned} &m\left[n\chi'''(0)+(n-4)\alpha^2\chi'(0)\right]\\ &-\left[\phi'''(0)-3\alpha^2\phi'(0)\right]\\ &+i\alpha Re\left[\left(c-\hat{u}(0)\right)\chi'(0)+\hat{u}_2'(0)\chi(0)\right]\\ &-i\alpha Re\left[\left(c-\hat{u}(0)\right)\phi'(0)+\hat{u}_1'(0)\phi(0)\right]\\ &=i\alpha Re\frac{\phi(0)}{c-\hat{u}(0)}\left[Fr+\alpha^2We\right] \end{aligned} \qquad (10)$$

where the Weber number We and the Froude number Fr are defined by

$$We=\frac{\sigma}{\rho_1 U_\infty^2 L^*}$$

$$Fr=\frac{L^*}{\rho_1 U_\infty^2}\left[\hat{p}_1'(0)-\hat{p}_2'(0)\right]$$

respectively. Note that in deriving these equations it was used that

$$\hat{u}_1(0)=\hat{u}_2(0)=\hat{u}(0)$$

which follows from the condition on the $O(\epsilon^0)$ continuity of the tangential velocity. Because of the zero pressure gradient in the x-direction, the second derivative of the primary flow equals zero at both sides of the interface. The normal stress equation was derived using equation (5). Note that the resulting normal stress interface condition differs from the one used by Özgen[7].

Boundary conditions at infinity

At infinity we have the conditions that the perturbation velocities should approach zero. Thus we find

$$\Phi(y)\to 0, \quad y\to\infty$$
$$\Phi'(y)\to 0, \quad y\to\infty$$

where ϕ is replaced by Φ.

Observation of the gas layer Blasius velocity profile indicates that above a certain location this profile has a 'nearly' constant x-component of the velocity and a small y-component of the velocity. This location will be called the virtual interface, denoted by y_i. Therefore, one may assume that above this location the Orr-Sommerfeld equation reduces to

$$\Phi^{iv}-[\alpha^2+\gamma^2]\Phi''+\alpha^2\gamma^2\Phi=0$$

with

$$\gamma^2=\alpha^2+i\alpha Re(1-c), \qquad \Re(\gamma)>0$$

This linear ordinary differential equation can be solved analytically using the boundary conditions at infinity, resulting in

$$\psi(y)=Ce^{-\alpha(y-y_i)}+De^{-\gamma(y-y_i)}$$

where y_i is the non-dimensional location of the virtual interface[6].

This method gives rise to the following four interface conditions at the virtual interface y_i

$$\Phi(y_i)-\phi(y_i)=0$$
$$\Phi'(y_i)-\phi'(y_i)=0$$

$$\Phi''(y_i)-\phi''(y_i)=0$$
$$\Phi'''(y_i)-\phi'''(y_i)=0$$

These conditions can easily be derived from equations (7)-(10) assuming $m=1$, $n=1$, $r=1$, $Fr=0$ and $We=0$. The two 'extra' interface conditions are used to determine the two constants C and D.

Energy distribution

The energy distribution of the disturbances throughout the layers may be computed by adding the equations which are obtained by multiplying the x-momentum equation of the secondary flow by the secondary flow velocity component in the x-direction and the y-momentum equation by the secondary flow velocity component in the y-direction, and averaging this equation over one wave-length λ.
For a non-Newtonian liquid one obtains

$$\frac{dE}{dt}=RS+PR+DI$$

where E is the perturbation kinetic energy given by

$$E=\frac{1}{2\lambda}\int_0^{\lambda}[\tilde{u}^2+\tilde{v}^2]dx$$

RS the rate of perturbation energy transfer from the primary flow to the secondary flow via the Reynolds stress

$$RS=\frac{1}{\lambda}\frac{d\hat{u}}{dy}\int_0^{\lambda}[-\tilde{u}\tilde{v}]dx$$

PR the pressure term given by

$$PR=-\frac{1}{\lambda r}\int_0^{\lambda}[\tilde{u}\frac{\partial\tilde{p}}{\partial x}+\tilde{v}\frac{\partial\tilde{p}}{\partial y}]dx$$

and DI the rate of viscous dissipation given by

$$DI=\frac{m}{\lambda Rer}\int_0^{\lambda}[(2-n)\tilde{u}\frac{\partial^2\tilde{u}}{\partial x^2}+n\tilde{u}\frac{\partial^2\tilde{u}}{\partial y^2}]dx$$
$$+\frac{m}{\lambda Rer}\int_0^{\lambda}[n\tilde{v}\frac{\partial^2\tilde{v}}{\partial x^2}+(2-n)\tilde{v}\frac{\partial^2\tilde{v}}{\partial y^2}]dx$$
$$+\frac{m(n-1)}{\lambda Rer}\int_0^{\lambda}[(\frac{d\hat{u}}{dy})^{-1}(\frac{d^2\hat{u}}{dy^2})(n\tilde{u}\frac{\partial\tilde{u}}{\partial y}+n\tilde{u}\frac{\partial\tilde{v}}{\partial x}+2\tilde{v}\frac{\partial\tilde{v}}{\partial y})]dx$$

where m, r and Re are defined according to equation (10).

Numerical solution

The method to solve the above set of two linear fourth-order differential equations including boundary conditions is described by Miesen & Boersma[6]. In this method the stream functions ϕ and χ are decomposed in a series of $N+1$ Chebyshev polynomials ($T_m(z)$)

$$\chi(z)=\sum_{m=0}^{N}a_mT_m(z)\qquad\phi(z)=\sum_{m=0}^{N}b_mT_m(z)$$

which are orthogonal on the interval [-1,1]. Here a_m and b_m are arbitrary complex constants. Employing a coordinate transformation in both layers to define the equation on the interval [-1,1], substituting the Chebyshev polynomials, imposing the equations at N-3 collocation points (the maxima of the Chebyshev polynomials) in both layers and applying the six boundary and four interface conditions, one gets a generalized matrix eigenvalue problem

$$A\underline{x}=cB\underline{x}$$

where $\underline{x}=[a_0,\ldots,a_N,b_0,\ldots,b_N,C,D]$, A and B are $(2N+4)$-matrices and c is the complex eigenvalue or wave speed. It should be noted that the equation describing continuity of tangential velocity was used to linearize the normal stress interface condition in c. The QZ-algorithm has been used to compute the $2N+4$ eigenvalues of the system. Prior to applying this algorithm, all rows of B containing only zeros are eliminated to avoid the introduction of infinite eigenvalues and to improve the accuracy of the computed eigenvalues.

Results

The case of a non-Newtonian power-law liquid sheared by a Newtonian gas [7](case: 4108200a) was used to perform the calculations. The effects of the surface tension and gravity have not been taken into account in the present calculations.
As can be seen from Figure 6, which shows $|c_N-c_{N-1}|$ as function of the number of Chebyshev polynomials N, the method shows exponential convergence. Here c_k is the largest eigenvalue obtained with k Chebyshev polynomials. For further calculations a number of 40 Chebyshev polynomials in both layers was judged adequate.
In the calculations two unstable modes were observed. The first mode is the so-called Blasius mode (see Figure 7 and 8), as it coincides with the curve obtained for pure Blasius flow. This mode is stable for a Reynolds number Re_{δ^*} below the critical Reynolds number of the Blasius boundary-layer flow.

Here Re_{δ^*} is the Reynolds number based on the displacement thickness δ^*.

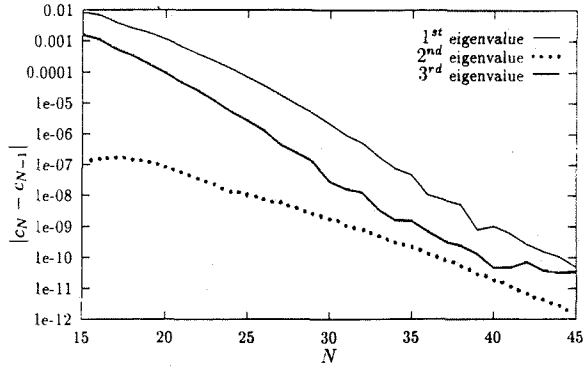

Figure 6: $|c_N-c_{N-1}|$ vs N: $y_i=10$, $y_*=0.86$, $\alpha=0.2$, $Re_{\delta^*}=1000$, $m=101908.3$, $n=0.82$, $r=1400$, $Fr=0$ and $We=0$

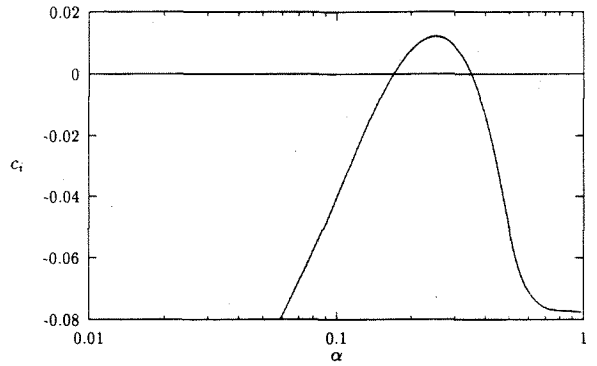

Figure 7: c_i vs α (Blasius mode): $y_i=10$, $y_*=0.86$, $Re_{\delta^*}=1000$, $m=101908.3$, $n=0.82$, $r=1400$, $Fr=0$, $We=0$ and $N=40$

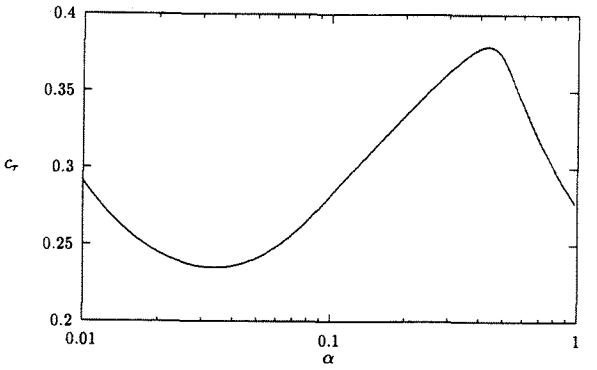

Figure 8: c_r vs α (Blasius mode): $y_i=10$, $y_*=0.86$, $Re_{\delta^*}=1000$, $m=101908.3$, $n=0.82$, $r=1400$, $Fr=0$, $We=0$ and $N=40$

The second mode is called the interfacial mode (see Figure 9 and 10). As this mode is absent in the Blasius boundary-layer flow, it is concluded that this mode originates from the presence of the liquid layer. For all Reynolds number Re_{δ^*} observed this mode has always unstable wave-numbers.

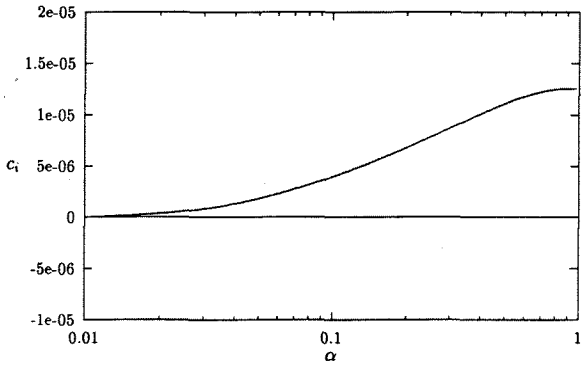

Figure 9: c_i vs α (Interfacial mode): $y_i=10$, $y_*=0.86$, $Re_{\delta^*}=1000$, $m=101908.3$, $n=0.82$, $r=1400$, $Fr=0$, $We=0$ and $N=40$

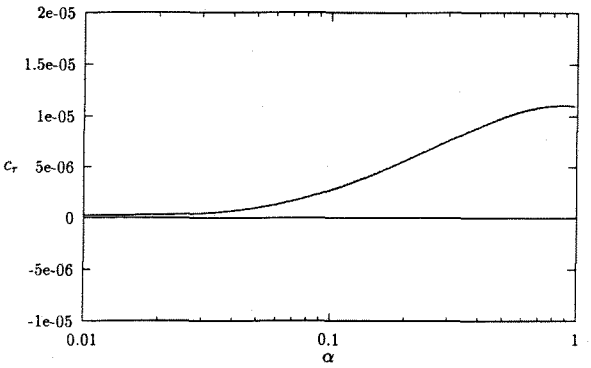

Figure 10: c_r vs α (Interfacial mode): $y_i=10$, $y_*=0.86$, $Re_{\delta^*}=1000$, $m=101908.3$, $n=0.82$, $r=1400$, $Fr=0$, $We=0$ and $N=40$

To investigate the Blasius mode further, the energy distribution of the secondary flow throughout the field was plotted in Figure 11 (Blasius flow) and Figure 12 (Blasius mode in two layer flow).
Both figures show that the energy distributions within the gas boundary-layer are similar. As the rate of change of kinetic energy is positive throughout the entire layer the mode is unstable. The instability is mainly caused by the action of the Reynolds stresses. Viscous dissipation has a stabilizing effect, the action of pressure, however, can have a stabilizing or a destabilizing effect depending on the y-location.

Conclusions

The linear hydrodynamic stability of the flow of a gas over a non-Newtonian power-law fluid has been investigated using the theory of small perturbations. The governing equations as well as the interface conditions have been derived. To take care of the boundary conditions at infinity a virtual interface has been introduced. A method using Chebyshev polynomials and the QZ-algorithm has been used to solve the resulting set of equations.
For the flow of air over an anti-icing fluid two

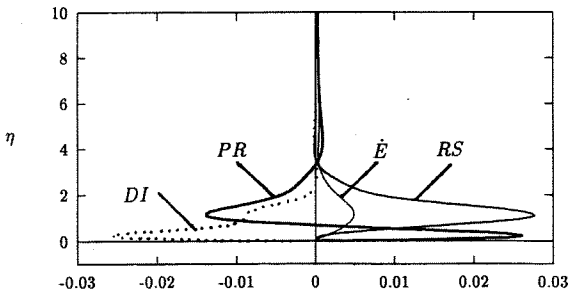

Figure 11: Energy distribution for Blasius flow: y_i=10, α=0.2, Re_ρ=1000 and N=40

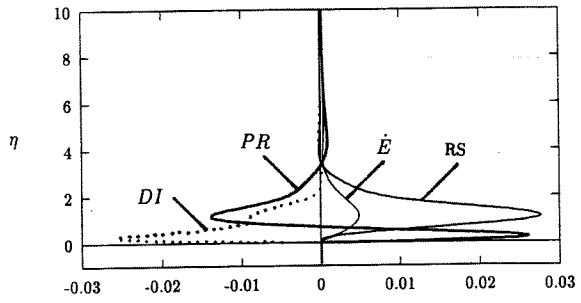

Figure 12: Energy distribution for Blasius mode: y_i=10, y_s=0.86, α=0.2, Re_ρ=1000, m=101908.3, n=0.82, r=1400, Fr=0, We=0 and N=40

unstable modes were obtained, i.e. the Blasius mode and the interfacial mode. The energy distribution of the perturbations was used to detect the origin of the instability. It was found that the Blasius instability was mainly caused by the action of the Reynolds stresses.

Instead of looking at the temporal instability one may also look at the spatial instability. This type of instability will be subject of future investigation for the present flow configuration. Furthermore attention will have to be paid to the non-linear growing phase following the initial linear phase.

Acknowledgements

This research has been carried out within the frame work of project DLR44.3298 of the Technology Foundation (Stichting voor de Technische Wetenschappen).

References

(1) Bradshaw, P., *Turbulence*, Topics in Applied Physics, Volume 12, 1976

(2) Carbonaro, M., *Aerodynamic effects of de-/anti-icing fluids and description of a facility and test technique for their assessment*, AGARD Conference Proceeding 496, Toulouse, France, 1991
republished with corrected data as:
Carbonaro M., Cunha F., *Aerodynamic effects of de-/anti-icing fluids and criteria for their aerodynamic acceptance*, SAE Aircraft Ground Deicing Conference & Exposition, Salt Lake City, June 15-17, 1993

(3) Drazin, P.G. and W.H. Reid, *Hydrodynamic stability*, Cambridge Monographs on Mechanics and Applied Mathematics. Cambridge University Press, Cambridge, Great Britain, 1981

(4) Hengst, J. van, *Aerodynamic effects of ground de-/anti-icing fluids on Fokker 50 and Fokker 100*, Journal of Aircraft, volume 30, number 1, 1993, pp. 35-40

(5) Loyd, B. and E.M. Murman, *Finite Volume Solution of the Compressible Boundary-Layer Equations*, NASA Contractor Report 4013, 1986

(6) Miesen, R. and B.-J. Boersma, *Hydrodynamic Stability of a Sheared Liquid Film*, J. Fluid Mech., vol. 301, 1995, pp. 175-202

(7) Özgen, S., *Stability of parallel non-Newtonian flows*, VKI Project Report 1995-22, 1995

(8) Runyan, L.J., T.A. Zierten, E.G. Hill and H.E. Addy, *Lewis Icing Research Tunnel Test of the Aerodynamic Effects of Aircraft Ground Deicing/Anti-icing Fluids*, NASA Technical Paper 3238, NASA Lewis Research Center, USA, 1992

(9) Wilcox, D.C., *Turbulence modelling for CFD*, DCW Industries, Inc., 1993

(10) Yih, C.-S., *Wave formation on a liquid layer for de-icing airplane wings*, J. Fluid Mech., vol. 212, 1990, pp. 41-53